3D STEERABLE WAVELETS AND MONOGENIC ANALYSIS FOR BIOIMAGING

Nicolas Chenouard[⋆†] *and Michael Unser*[⋆]

[⋆]Biomedical Imaging Group (BIG), École polytechnique fédérale de Lausanne (EPFL)
[†]Center for Biomedical Imaging (CIBM), Université de Lausanne (UNIL)

ABSTRACT

In this paper we introduce a 3D wavelet frame that has the key property of steerability. The proposed wavelet frame relies on the combination of a 3D isotropic wavelet transform with the 3D Riesz operator which brings steerability to the pyramid. The novel transform enjoys self reversibility and exact steering of the basis functions in any 3D direction by linear combination of the primary coefficients. We exploit the link between the Riesz transform and the directional Hilbert transform to define a multiresolution monogenic signal analysis in 3D which achieves multiscale AM/FM signal decomposition. We give an example of application of the 3D monogenic wavelet frame in biological imaging with the enhancement of anisotropic structures in 3D fluorescence microscopy.

Index Terms— 3D wavelet transform, Riesz transform, steerability, feature enhancement, monogenic signal

1. INTRODUCTION

Steerability is the ability to compute the response to a multidimensional directional filter as an angle-dependent linear combination of filterbank outputs. Freeman and Adelson pionneered the study of steerable filters with a filterbank consisting of a derivative of Gaussian filter which is rotated to a finite number of equi-spaced angles [1]. Simoncelli and colleagues soon after extended the steerability principles to 2D wavelet filterbanks [2]. The key idea of the so-called steerable pyramid is to apply a steerable and reversible filterbank to coefficients provided by an isotropic wavelet pyramid. The main benefits of the approach are three-fold: the pyramid is self-reversible, multiresolution is achieved, and the rotation-covariant property is inherited from the steerable filterbank, hence yielding straightforward rotation of the wavelet functions.

The steerability principles, as defined by Freeman and Adelson, is extendable to three dimensions when using 3D polar separable filters such as the derivatives of Gaussian. By contrast, it seems much harder to transpose the Simoncelli's design to 3D since the invertibility of the pyramid imposes some strict constraints on the filter design (i.e., equiangular tiling of the frequency sphere). Designing 3D steerable wavelets with perfect reconstruction properties would however make possible numerous novel image-processing techniques relying on directional analysis.

In this paper, we present a 3D steerable wavelet frame. Our approach relies on the Riesz transform which can be used to map any wavelet frame of $L_2(\mathbb{R}^3)$ into a directional wavelet frame of the same space [3]. This powerful property has been already exploited to design 2D steerable filterbanks [3]. Moreover, the theoretical basis for steerable wavelets in high-dimensional space has been recently investigated [4, 5]. We focus in this paper on the 3D case which is particularly important for bioimaging. We apply the 3D Riesz operator to the output of an isotropic wavelet pyramid such that the whole directionality information is conveyed by the Riesz transform. By doing so, the resulting Riesz-wavelet frame inherits the steerability property of the Riesz transform. We discuss its self-reversible filterbank implementation and the coefficient-steering process.

It has been previously highlighted that the Riesz transform can be viewed as the natural multidimensional extension of the Hilbert transform [6]. This link has been exploited in 2D to define a multiscale analytical signal called the monogenic wavelet [3]. The monogenic wavelet is an extension of the 1D analytical signal [7], and thus gives access to key AM/FM parameters of the image. More recently, a monogenic signal in high-dimensional space has been defined thanks to a Clifford algebra formalism [4]. In this paper we propose a 3D counterpart to the monogenic wavelet proposed in [3]. We are able to suggest a more intuitive interpretation than the Clifford algebra formalism when considering the link between the 3D Riesz-wavelet transform and the Hilbert transform along a 3D direction. For each wavelet location, we derive a regularized local orientation, the coherency (i.e., the degree of directionality) of the neighborhood, and some AM/FM parameters.

In biomaging, we argue that the multiscale monogenic parameters are good descriptors of the underlying biological structure. Indeed, biological environments often contain highly directional features in 3D, such as filaments, dendrites, or membranes. As a consequence, the 3D monogenic wavelet analysis can be exploited to drive the processing of 3D microscopy images. In the last part, we give an example the enhancement of anisotropic structures in fluorescence microscopy which takes advantage of the proposed method.

2. 3D RIESZ-WAVELET TRANSFORM

2.1. 3D Riesz Transform

In the sequel, we discuss the transformation of finite-energy functions $f(\boldsymbol{x}) \in L_2(\mathbb{R}^3)$ with $\boldsymbol{x} = (x_1, x_2, x_3) \in \mathbb{R}^3$. The Fourier transform of the input signal $f(\boldsymbol{x})$ is $\hat{f}(\boldsymbol{\omega}) = \int_{\mathbb{R}^3} f(\boldsymbol{x}) \mathrm{e}^{-j\langle \boldsymbol{\omega}, \boldsymbol{x}\rangle} \mathrm{d}\boldsymbol{x}$, with $j = \sqrt{-1}$ and $\boldsymbol{\omega} = (\omega_1, \omega_2, \omega_3)$ the 3D pulsation vector.

The Riesz transform of a function $f(\boldsymbol{x})$ of $L_2(\mathbb{R}^3)$ is the scalar-to-vector transformation

$$\boldsymbol{\mathcal{R}} f(\boldsymbol{x}) = \begin{pmatrix} \mathcal{R}_1 f(\boldsymbol{x}) \\ \mathcal{R}_2 f(\boldsymbol{x}) \\ \mathcal{R}_3 f(\boldsymbol{x}) \end{pmatrix}$$

The Riesz operator component $\mathcal{R}_i$ is linear, space-invariant, and characterized by the frequency response

$$\widehat{\mathcal{R}_i f}(\boldsymbol{\omega}) = -j \frac{\omega_i}{||\boldsymbol{\omega}||} \hat{f}(\boldsymbol{\omega}). \quad (1)$$

The Fourier-domain definition of the Riesz transform highlights that $\boldsymbol{\mathcal{R}} f$ can be viewed as the 3D gradient vector of the Laplacian

of order $-1/2$ (an isotropic smoothing operator) of f: $\boldsymbol{\mathcal{R}} f = -\boldsymbol{\nabla}\boldsymbol{\Delta}^{-1/2} f$. Let's indeed recall the Fourier-domain definition of these operators: $\boldsymbol{\nabla} \overset{\mathcal{F}}{\longleftrightarrow} j\boldsymbol{\omega}$ and $\boldsymbol{\Delta}^{-1/2} \overset{\mathcal{F}}{\longleftrightarrow} ||\boldsymbol{\omega}||^{-1}$. Unlike the usual gradient $\boldsymbol{\nabla}$, the Riesz transform is self-reversible

$$\widehat{\boldsymbol{\mathcal{R}}^{\star}\boldsymbol{\mathcal{R}}} f(\boldsymbol{\omega}) = \frac{(j\boldsymbol{\omega})^{*}(j\boldsymbol{\omega})}{||\boldsymbol{\omega}||^{2}} \hat{f}(\boldsymbol{\omega}) = \hat{f}(\boldsymbol{\omega}).$$

This allows us to define a self-invertible wavelet frame of $L_2(\mathbb{R}^3)$ (tight frame). We however see that there exists a singularity for the frequency $(0, 0, 0)$. This issue will be fixed later, thanks to the vanishing moments of the primary wavelet transform.

2.2. Steerability

The interpretation of the Riesz transform as being a directional derivative filterbank makes its steerability easy to understand: it behaves similarly to a steerable gradient filterbank, with the added crucial property of perfect reconstruction. We parameterize any rotation in 3D with a real and unique 3 by 3 matrix $\mathbf{U}$ which is unitary ($\mathbf{U}^T\mathbf{U} = \mathbf{I}$). Let us consider the Fourier transform of the impulse response of the Riesz transform after a rotation by $\mathbf{U}$ as

$$\boldsymbol{\mathcal{R}}\widehat{\{\delta\}(\mathbf{U}\boldsymbol{x})}(\boldsymbol{\omega}) = -j\frac{\mathbf{U}\boldsymbol{\omega}}{||\mathbf{U}\boldsymbol{\omega}||} = \mathbf{U}\left(-j\frac{\boldsymbol{\omega}}{||\boldsymbol{\omega}||}\right) = \mathbf{U}\widehat{\boldsymbol{\mathcal{R}}\{\delta\}(\boldsymbol{x})}(\boldsymbol{\omega}),$$

with δ the Dirac distribution. The rotated Riesz transform of f therefore corresponds to the multiplication by $\mathbf{U}$ of the non-rotated Riesz coefficients

$$\boldsymbol{\mathcal{R}}_{\mathbf{U}} f(\boldsymbol{x}) = \mathbf{U}\boldsymbol{\mathcal{R}} f(\boldsymbol{x}), \tag{2}$$

which demonstrates the 3D steerability of the Riesz transform.

2.3. Riesz-Wavelet Pyramid

One crucial property of the Riesz transform is its ability to map any frame of $L_2(\mathbb{R}^3)$ (in particular wavelet frames) into $L_2(\mathbb{R}^3)$ since it preserves the inner product of $L_2(\mathbb{R}^3)$ [3, 4]. Following the previous Riesz-wavelet constructions [3, 4], we propose to apply the 3D Riesz transform to the coefficients of a wavelet pyramid to build a steerable wavelet transform in 3D.

2.3.1. Primary Wavelet pyramid

A primary isotropic wavelet pyramid is required in order to preserve the relevance of the directional analysis performed by the Riesz transform. Moreover, the bandlimitedness of the wavelet bands must be enforced to ensure the isotropy of the primary wavelet together with the possibility of down-sampling [1, 8]. A conventional orthogonal and separable wavelet transform fulfills none of these conditions. In [3], a 2D spline-based wavelet transform was used as the primary transform. However, while low-order spline wavelets are fast to compute, they are not truly isotropic. We thus propose instead a 3D non-separable wavelet with an isotropic wavelet function, as done in 2D in [2]. To achieve bandlimitedness of the wavelet bands it is more convenient to design the wavelet transform directly in the 3D Fourier domain. Moreover, the isotropy constraint imposes a purely radial wavelet function (i.e., it depends on $||\boldsymbol{\omega}||$ and not on the individual frequency components ω_i in the Fourier domain). Among all possible wavelet functions, two are of particular interest: the Shannon's wavelet

$$\hat{\psi}_{sha}(\omega) = \begin{cases} 1, & \frac{\pi}{2} \leq ||\omega|| \leq \pi \\ 0, & \text{otherwise} \end{cases}$$

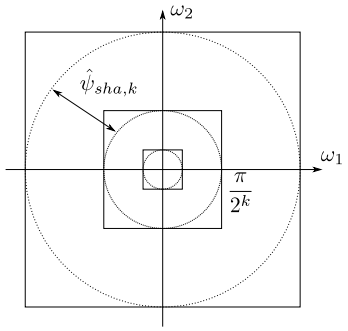

Fig. 1. Frequency tiling with the Shannon's wavelet. Each wavelet scale is obtained by a bandpass filter of support $[\pi/2^{k+1}, \pi/2^k]$. The space-domain subsampling operations, which restrict the frequency plane to the support of each wavelet function, are shown with boxes.

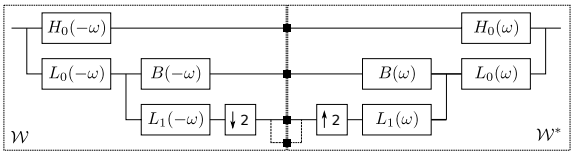

(a) Filterbank implementation of the isotropic wavelet transform. A cascade of low-pass filters ($L_i(\boldsymbol{\omega})$) and high-pass filters ($H_0(\boldsymbol{\omega})$ and $B(\boldsymbol{\omega})$) is applied. The filterbank is self-reversible.

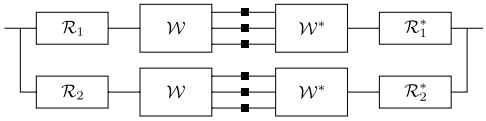

(b) Self-reversible Riesz-wavelet filterbank.

Fig. 2. The Riesz-wavelet transform filterbank implementation.

and the Simoncelli's wavelet used for the 2D steerable pyramid

$$\hat{\psi}_{sim}(\omega) = \begin{cases} \cos\left(\frac{\pi}{2}\log_2\left(\frac{2||\omega||}{\pi}\right)\right), & \frac{\pi}{4} < ||\omega|| \leq \pi \\ 0, & \text{otherwise.} \end{cases}$$

The Shannon's wavelet function is a radial step function which corresponds to the frequency-domain tiling shown in Fig. 1. This wavelet transform decomposes the signal spectrum with isotropic and non-overlapping tiles. Using the Simoncelli's wavelet function would result in a smooth frequency partitioning with overlapping tiles, which is less prone to reconstruction artifacts after coefficient processing. The decomposition shown in Figure 1 can be efficiently achieved by a succession of filtering and downsampling operations, the high-pass coefficient remaining non-subsampled to alleviate aliasing, as opposed to the orthogonal wavelet transform. The wavelet decomposition cascade is illustrated in Figure 2(a).

2.3.2. Riesz-Wavelet Pyramid

We build a Riesz-wavelet frame by applying the Riesz transform to each scale of the isotropic pyramid defined by the wavelet function and its dual $\{\psi, \tilde{\psi}\}$. The continuous version of the Riesz-wavelet transform prior subsampling is

$$q_k(\boldsymbol{x}) = \boldsymbol{\mathcal{R}}\{\psi_k * f\}(\boldsymbol{x})$$

for k going from 1 to K, where K is the finest wavelet scale. The function $f(\boldsymbol{x})$ can be exactly reconstructed by inverting the Riesz transform and the subsampled wavelet pyramid

$$\sum_{k=1}^{K} \boldsymbol{\mathcal{R}}^* \{q_k\} * \tilde{\psi}_k(\boldsymbol{x}) = \sum_{k=1}^{K} \boldsymbol{\mathcal{R}}^* \boldsymbol{\mathcal{R}} \{\psi_k * f\} * \tilde{\psi}_k(\boldsymbol{x}) = \sum_{k=1}^{K} \psi_k * f * \tilde{\psi}_k(\boldsymbol{x}) = f(\boldsymbol{x}).$$

since the $\psi_k(\boldsymbol{x})$ are bandlimited. It is worth noting here that the wavelet functions we use have at least one null moment (i.e., $\hat{\psi}_k((0,0,0)) = 0$). The singularity of the Riesz transform at the origin is therefore tempered by the wavelet transform and is now harmless. Moreover, the Riesz and wavelet transforms can be commuted. We give in Fig. 2(b) a filterbank implementation of the Riesz-wavelet transform in which the wavelet decomposition is applied to the Riesz coefficients.

The primary wavelet function being isotropic, the directionality information is conveyed at each scale by the Riesz transform only. The Riesz-wavelet coefficients can thus be steered in the same way as the 3D Riesz coefficients (2). Specifically, the coefficients $q_{k,\mathbf{U}}(\boldsymbol{x})$ that correspond to a rotation of the Riesz-wavelet atoms by the unitary matrix $\mathbf{U}$ are computed as

$$q_{k,\mathbf{U}}(\boldsymbol{x}) = \boldsymbol{\mathcal{R}}_{\mathbf{U}} \{\psi_k * f\}(\boldsymbol{x}) = \mathbf{U} q_k(\boldsymbol{x}).$$

3. MONOGENIC WAVELET ANALYSIS

The analytic signal was introduced by Gabor [7] as a complex extension of a 1-D signal

$$f_{anal}(x) = f(x) + j\mathcal{H}f(x) = A(x)\mathrm{e}^{j\xi(x)}$$

based upon the Hilbert transform $\mathcal{H}$ which is the linear and shift-invariant operator that maps all 1D cosine functions into their corresponding sine functions. An AM/FM signal analysis is achieved with this representation by taking the time-varying amplitude as $A(x) = |f_{anal}(x)|$ and the instantaneous frequency as $\nu(x) = \mathrm{d}\xi(x)/\mathrm{d}x$. One extension of the analytical signal to 2D is via the Riesz transform [6] which can be viewed as a natural extension of the Hilbert transform to multiple dimensions. The so-called *monogenic signal* was recently extended to the analysis of 2D Riesz-wavelet coefficients [3, 4]. We present here a 3D monogenic wavelet analysis.

3.1. 3D Monogenic Signal

We propose to perform a 1D AM/FM signal analysis, like for the analytical signal, but along a 3D direction. In particular, we choose the vector $\boldsymbol{u}$ with $||\boldsymbol{u}|| = 1$ as the local orientation that maximizes the directional Hilbert-transform response. (We present in the next section a fast and robust way to compute $\boldsymbol{u}$.) When comparing the frequency response of the Hilbert transform ($\widehat{\mathcal{H}f}(\omega) = -j\omega/|\omega|\hat{f}(\boldsymbol{\omega})$) with the Fourier-domain definition of the Riesz components (1), it is apparent that $\mathcal{H}_{\boldsymbol{u}}$, which is the Hilbert transform along the direction $\boldsymbol{u}$, corresponds to the projection of the Riesz transform onto $\boldsymbol{u}$: $\mathcal{H}_{\boldsymbol{u}} = \boldsymbol{u}^T \boldsymbol{\mathcal{R}}$. We thus build a 3D extension of the monogenic signal which is based on the 3D Riesz transform

$$\mathbf{f}_{mono}(\boldsymbol{x}) = (f(\boldsymbol{x}), \mathcal{R}_1 f(\boldsymbol{x}), \mathcal{R}_2 f(\boldsymbol{x}), \mathcal{R}_3 f(\boldsymbol{x})) = (f(\boldsymbol{x}), f_1(\boldsymbol{x}), f_2(\boldsymbol{x}), f_3(\boldsymbol{x})).$$

We compute the local signal amplitude (AM component) as $A(\boldsymbol{x}) = ||\mathbf{f}_m(\boldsymbol{x})||$. The local phase ξ in the direction $\boldsymbol{u}$ is computed as $\xi(\boldsymbol{x}) = \arctan\left(\mathcal{H}_{\boldsymbol{u}}(\boldsymbol{x})/f(\boldsymbol{x})\right) = \arctan\left(\boldsymbol{u}^T \boldsymbol{\mathcal{R}} f(\boldsymbol{x})/f(\boldsymbol{x})\right)$.

3.2. Tensor-Based Estimation of the Local Orientation

We extend to 3D the local orientation estimation procedure proposed in [3] that relies on the structure tensor [9]. We select the orientation $\boldsymbol{u}$ which maximizes $\mathcal{H}_{\boldsymbol{u}}(\boldsymbol{x})$, but, instead of doing it pointwise, we optimize the response over a 3D local neighborhood that is specified by the isotropic and positive weighting function $v(\boldsymbol{x})$. The function $v(\boldsymbol{x})$ is typically a 3D Gaussian window which acts as a regularization function of the orientation map. The pointwise optimization problem is

$$\boldsymbol{u}_v(\boldsymbol{x}_0) = \arg \max_{||\boldsymbol{u}||=1} \int_{\mathbb{R}^3} v(\boldsymbol{x} - \boldsymbol{x}_0) |\mathcal{H}_{\boldsymbol{u}} f(\boldsymbol{x})|^2 \mathrm{d}\boldsymbol{x}.$$

Exploiting the link between the directional Hilbert transform and the Riesz transform, and exploiting the steerability of the latter, we write

$$|\mathcal{H}_{\boldsymbol{u}} f(\boldsymbol{x})|^2 = \left(\boldsymbol{u}^T \boldsymbol{\mathcal{R}} f(\boldsymbol{x})\right) \left(\boldsymbol{u}^T \boldsymbol{\mathcal{R}} f(\boldsymbol{x})\right)^* = \boldsymbol{u}^T (\boldsymbol{\mathcal{R}} f(\boldsymbol{x}))(\boldsymbol{\mathcal{R}} f(\boldsymbol{x}))^* \boldsymbol{u}.$$

which shows that estimating the local orientation is a quadratic form maximization problem which turns out to be a standard eigenvalue problem. The vector $\boldsymbol{u}$ is computed pointwise as the eigenvector corresponding to the largest eigenvalue of the tensor matrix $\mathbf{J}(\boldsymbol{x}_0)$, with

$$[\mathbf{J}(\boldsymbol{x_0})]_{mn} = \int v(\boldsymbol{x} - \boldsymbol{x}_0) f_m(\boldsymbol{x}) f_n(\boldsymbol{x}) \mathrm{d}\boldsymbol{x}$$

and $m, n \in \{1, 2, 3\}$. The sorted collection of eigenvectors of $\mathbf{J}(\boldsymbol{x}_0)$ defines a rotation matrix $\mathbf{U}_v$ such that the energy of the first band of the rotated Riesz transform $\mathbf{U}_v \boldsymbol{\mathcal{R}} f$ is maximized since $[\mathbf{U}_v]_1 = \boldsymbol{u}_v^T$. The second band of $\mathbf{U}_v \boldsymbol{\mathcal{R}} f$ contains the maximal amount of the residual energy of the transformed signal.

The eigenvalue decomposition of $\mathbf{J}(\boldsymbol{x}_0)$ also allows us to quantify the degree of directionality of the neighborhood through the relative weights of the eigenvalues. We define the coherency of the 3D local neighborhood as

$$\chi(\boldsymbol{x}_0) = \frac{\lambda_1 - (\lambda_2 + \lambda_3)/2}{\lambda_1 + (\lambda_2 + \lambda_3)/2},$$

which takes the value 1 when all the eigenvalues except the first one do vanish (the energy is concentrated along the $\boldsymbol{u}$ direction), and 0 when the three eigenvalues are equal (isotropic gradient values).

3.3. 3D Monogenic Wavelet

We apply the 3D monogenic analysis to each scale of the 3D isotropic wavelet pyramid described above, resulting in the multiscale monogenic signal

$$\mathbf{f}_{mono,k}(\boldsymbol{x}) = (\psi_k * f(\boldsymbol{x}), \mathcal{R}_1\{\psi_k * f\}(\boldsymbol{x}), \mathcal{R}_2\{\psi_k * f\}(\boldsymbol{x}), \mathcal{R}_3\{\psi_k * f\}(\boldsymbol{x}))$$

with $k = 1 \ldots K$. The isotropy of the primary wavelet pyramid is crucial here because the directional analysis relies on the Riesz channels.

4. MICROSCOPY IMAGE ANALYSIS AND PROCESSING

We show in Fig. 3 the principal directions obtained by the monogenic Riesz-wavelet transform for fluorescence images of collagen filaments. The figure is an illustration of the ability of our method to

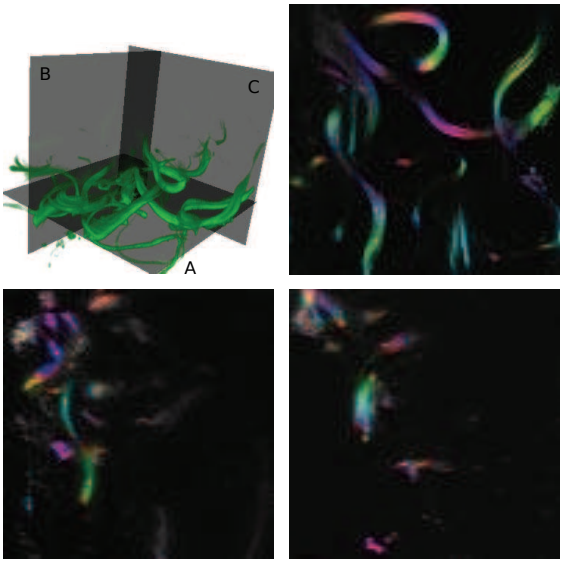

Fig. 3. Top-Left: a 3D image stack of collagen filaments. From top-right to bottom-right: color encoded (hue) monogenic direction for the plans A, B and C, after an orthogonal projection onto the xy, xz and yz plans, respectively. The saturation indicates the value of the local coherency.

estimate in a robust and consistent manner the local 3D orientation in microscopy images.

The monogenic parameters can be further exploited to drive processing techniques which self adapt to the local features. For instance, a multiscale monogenic signal has been exploited to identify feature points in various 2D medical images [10]. We propose here an adaptive anisotropic smoothing technique which consists in steering the Riesz-wavelet coefficients according to the monogenic directions $\mathbf{U}_v$, thresholding them, and reconstructing a smoothed image by inverting the Riesz-wavelet pyramid. Steering the coefficients according to $\mathbf{U}_v$ yields an increased response in the first Riesz channel since it corresponds to the main local orientation. We have applied a soft-threshold independently to each channel, resulting in a strong smoothing of the features which are orthogonal to the main local orientation. As shown in Fig. 4, the proposed technique is able to smooth the image while preserving the diectional features, which is beneficial to the iso-surface visualization in 3D of the filaments.

5. CONCLUSION

We have introduced a 3D steerable wavelet transform. The proposed wavelet frame relies on the combination of an isotropic nonseparable wavelet pyramid and the 3D Riesz transform. We have described a Fourier-domain implementation of the transform which is achieved thanks to a fast and self-reversible filterbank. Among the interesting properties of the Riesz-wavelet transform, two are of main interest: its steerability, and its link with the directional Hilbert transform. The latter is the basis for the design of a 3D monogenic wavelet transform that allows the directional AM/FM analysis of 3D images. We have given an example of 3D biological image processing for which the proposed techniques are beneficial.

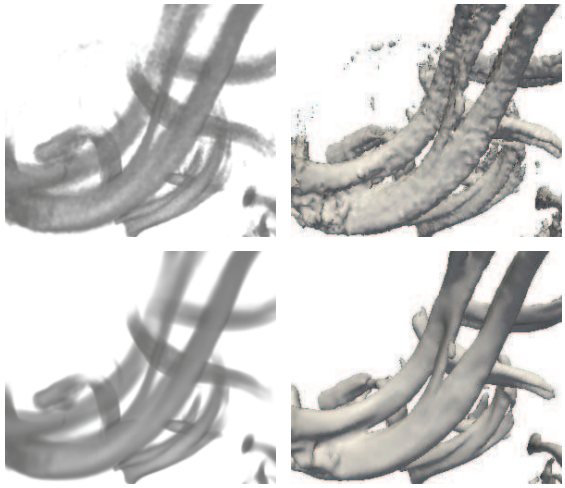

Fig. 4. Top-row: 3D original fluoescence image of collagen filaments and its iso-surface representation; Bottom-row: Anisotropic feature enhancement image and its iso-surface representation.

6. REFERENCES

[1] W.T. Freeman and E.H. Adelson, "The design and use of steerable filters," *Trans. Pattern Anal. and Machine Int.*, vol. 13, no. 9, pp. 891 –906, Sep. 1991.

[2] A. Karasaridis and E. Simoncelli, "A filter design technique for steerable pyramid image transforms," in *IEEE ICASSP*, 7-10 1996, vol. 4, pp. 2387–2390.

[3] M. Unser, D. Sage, and D. Van De Ville, "Multiresolution monogenic signal analysis using the Riesz-Laplace wavelet transform," *Trans. Img. Proc.*, vol. 18, no. 11, pp. 2402–2418, Nov. 2009.

[4] S. Held, M. Storath, P. Massopust, and B. Forster, "Steerable wavelet frames based on the riesz transform," *Trans. Img. Proc.*, vol. 19, no. 3, pp. 653 –667, Mar. 2010.

[5] M. Unser and D. Van De Ville, "Wavelet steerability and the higher-order Riesz transform," *Trans. on Img. Proc.*, vol. 19, no. 3, pp. 636–652, Mar. 2010.

[6] M. Felsberg and G. Sommer, "The monogenic signal," *Trans. Sig. Proc.*, vol. 49, no. 12, pp. 3136 –3144, Dec. 2001.

[7] D. Gabor, "Theory of communications," *J. Inst. Elect. Eng.*, vol. 93, no. 3, pp. 429–457, 1946.

[8] J. R. Romero, S. K. Alexander, S. Baid, S. Jain, and M. Papadakis, "The geometry and the analytic properties of isotropic multiresolution analysis," *Adv. Comput. Math.*, vol. 31, no. 1-3, pp. 283–328, 2009.

[9] B. Jähne, *Digital image processing*, New York: Springer, 2005.

[10] T. Szilagyi and M. Brady, "Feature extraction from cancer images using local phase congruency: A reliable source of image descriptors," in *IEEE ISBI*, jun. 2009, pp. 1219 –1222.